

# When Latent Geometry Is Not Enough: Draft-Conditioned Latent Refinement for Non-Autoregressive Text Generation

De Shuai Zhang

Beijing Wuzi University

Technical Report v1, May 2026

*Stage 1 (latent autoencoder and DraftPrior diagnostics) complete.*

## Abstract

Continuous diffusion and flow models are attractive for non-autoregressive text generation because they can update all positions in parallel. A major difficulty is the interface between continuous latent states and discrete tokens. This report studies a draft-conditioned latent refinement model built from a frozen BERT encoder, a parallel decoder, a denoising DraftPrior, a local FlowNet, and a learned diagonal MetricNet. Early Gaussian-start experiments showed that good latent-space metrics, such as scale matching or cosine similarity, do not guarantee good decoding. Generated latents can be close to real encoder latents but still produce high-entropy, biased, or repetitive token distributions. We therefore frame the task as controlled local refinement rather than full generation from noise. On ROCStories, using the first two sentences as prompt and the last three as target, full 768-dimensional BERT latents recover tokens much better than compressed 256-dimensional latents. With 768-dimensional latents, DraftPrior target-token probability is 0.938 for clean drafts, 0.613 for 3% token dropout, 0.483 for 5% dropout, and 0.272 for 10% dropout. Local flow refinement and fused decoder-aware readout give modest additional gains, while metric learning and OT-style alignment improve geometry but do not close the decoder gap. The main result is a diagnostic one: latent geometry alone is not enough. Continuous latent text generation should be evaluated by decoder recoverability, the quality of the start distribution, and whether refinement preserves decoder-readable structure.

**Keywords:** flow matching, Riemannian flow, non-autoregressive text generation, latent text generation, draft refinement, BERT autoencoder, decoder recoverability

## 1 Introduction

Autoregressive language models based on Transformer architectures [1], including GPT-style systems [3], generate one token at a time. This factorization is powerful, but it makes generation sequential. Non-autoregressive generation is attractive because it could produce an entire continuation in parallel and permit global sequence-level refinement. The difficulty is that language is discrete, while diffusion and flow-based methods operate naturally in continuous spaces.

A common approach, related to denoising autoencoding models such as BART [4], is to encode text into a continuous latent sequence, generate or refine in that latent space, and decode the resulting latents back into tokens. This resembles latent diffusion in vision, but the text setting is

less tolerant. In images, a slightly imperfect latent may still decode into a plausible image. In text, a small latent error can change the token identity completely or leave the decoder uncertain across many vocabulary items.

This project began as a conditional latent flow-matching system. A frozen BERT encoder [2] maps an input token sequence  $x = (x_1, \dots, x_n)$  of length  $n$  into continuous latent representations through a projection layer  $P$ :

$$z = P(E_{\text{BERT}}(x)), \quad z \in \mathbb{R}^{n \times d} \quad (1)$$

where  $d$  is the latent dimension ( $d = 768$  in our main experiments,  $d = 256$  for the compressed baseline). A parallel decoder  $p_\phi$  predicts all token distributions simultaneously, forming a stage-1 latent autoencoder trained with:

$$\mathcal{L}_{\text{AE}} = - \sum_{i=1}^n \log p_\phi(x_i | z) \quad (2)$$

For conditional generation, the latent sequence is split into prompt and suffix parts at position  $m$ :

$$z = (z^p, z^s), \quad z^p = z_{1:m}, \quad z^s = z_{m+1:n} \quad (3)$$

where  $z^p \in \mathbb{R}^{m \times d}$  is the known prompt latent and  $z^s \in \mathbb{R}^{(n-m) \times d}$  is the suffix latent to be generated. In our ROCStories experiments,  $m = 32$  prompt token slots and  $n - m = 32$  suffix token slots.

Diagnostics showed that the original Gaussian-start formulation was too optimistic. A flow path interpolates between noise and the real suffix latent:

$$z_0 \sim \mathcal{N}(0, I), \quad z_t = (1 - t)z_0 + tz^s, \quad t \sim \mathcal{U}(0, 1) \quad (4)$$

where  $I$  is the identity matrix and  $t$  is the interpolation timestep. A FlowNet  $v_\theta$  is trained to predict the target velocity  $u_t = z^s - z_0$ :

$$\mathcal{L}_{\text{FM}} = \mathbb{E} [\|v_\theta(z_t, t, z^p) - (z^s - z_0)\|^2] \quad (5)$$

The flow could improve latent-space metrics while the decoder still produced high-frequency-token attractors, repetition, and poor target-token probability. Specifically, generated latents  $\hat{z}^s$  could achieve high cosine similarity with real suffix latents while still decoding poorly:

$$\cos(z^s, \hat{z}^s) \approx 1 \not\Rightarrow P_{\text{target}}(\hat{z}^s) \text{ is high} \quad (6)$$

where  $P_{\text{target}}$  is the average target-token probability under the frozen decoder, defined formally in Eq. 40.

The current version reframes the system. Instead of asking a flow to create a valid text continuation from pure noise, we use a rough draft as an instance-level guide. The draft is encoded into the same latent space, a DraftPrior maps it toward the decoder-readable basin, and the metric-aware flow applies only a small local correction. This report studies that controlled refinement setting and the failure modes that remain.

## 1.1 Contributions

This report makes four contributions:

- We identify a decoder recoverability failure mode: latent similarity does not guarantee token recovery.

- We introduce a draft-conditioned refinement setup for ROCStories, using the first two sentences as prompt and the last three as target.
- We compare 256-dimensional compressed latents with full 768-dimensional BERT latents and show that stronger compression loses token-level information.
- We ablate DraftPrior, local FlowNet refinement, MetricNet, OT-style alignment, fused readout, and bounded residual refinement. The start distribution gives most of the recoverability; geometry-based refinement gives smaller gains.

## 2 Related Work

### 2.1 Continuous diffusion and flow models for text

Diffusion-LM [19], building on diffusion models such as DDPM [13] and score-based generative modeling [14] — which learns the score function  $s_\theta(x_t, t) \approx \nabla_{x_t} \log p(x_t)$  and generates samples via Langevin dynamics — demonstrated that continuous diffusion can be adapted to text by mapping words into continuous embeddings and then rounding back to tokens. Its treatment of embedding choice and rounding is directly relevant here: the continuous-to-discrete interface is not an implementation detail, but a central modeling problem. In this report, the rounding operation is replaced by a parallel decoder, but the same challenge remains: generated continuous states must land in regions that the decoder can reliably map to tokens.

Diffusion-LM addresses the continuous-to-discrete gap with a clamping trick: during sampling, the predicted clean vector  $f_\theta(\mathbf{x}_t, t)$  is mapped to its nearest word-embedding sequence before forming the next denoising state,

$$\mathbf{x}_{t-1} = \sqrt{\bar{\alpha}_t} \text{Clamp}(f_\theta(\mathbf{x}_t, t)) + \sqrt{1 - \bar{\alpha}_t} \epsilon. \quad (7)$$

Our system faces the same interface problem, but uses a different constraint. Rather than snapping intermediate states to discrete word embeddings, we start from a decoder-readable draft latent and restrict the refinement magnitude:

$$\mathbf{z}_{\text{res}} = \mathbf{z}_{\text{ode}} + \lambda \tanh R_\omega(\mathbf{z}_{\text{ode}}, \mathbf{z}^p) \quad (8)$$

where  $\lambda > 0$  is a scalar bound controlling the maximum refinement magnitude, ensuring  $\|\mathbf{z}_{\text{res}} - \mathbf{z}_{\text{ode}}\|_\infty \leq \lambda$ . Thus, Diffusion-LM enforces discreteness by repeated projection to the embedding vocabulary, while our bounded residual preserves local decoder-readability by preventing the refinement trajectory from moving too far from the draft-conditioned latent basin. These are analogous design responses to the same continuous-to-discrete problem, operating at different stages of generation.

Latent Diffusion for Language Generation [20] is especially close to our setting because it trains continuous generative models in the latent space of a language autoencoder and decodes sampled latent states back into natural language. Our system shares this latent-space generative view but differs in three important ways. First, we use a flow-based model rather than diffusion, updating the full suffix latent sequence jointly in parallel. Second, we replace the pretrained autoregressive decoder with a parallel decoder trained from scratch, removing left-to-right token conditioning during decoding. Third, this setting reveals a sharp decoder-readability failure mode: generated latents can be geometrically close to real suffix latents while still decoding poorly under a frozen parallel decoder. In our experiments, direct Gaussian-start latent generation was therefore insufficient, leading us to

adopt draft-conditioned local refinement, which begins from a structured decoder-readable latent state rather than pure noise.

DiffusionBERT [21] provides another relevant contrast: it trains BERT directly as the denoising model in a discrete diffusion process over token space, making BERT itself the generative component. Our system inverts this relationship — BERT is a frozen encoder that defines the latent space, while generation and decoding are handled by separate learned components operating in continuous space. Where DiffusionBERT asks how diffusion can improve masked language model generation, we ask whether continuously generated latents can be reliably decoded by a parallel decoder — a question that does not arise in discrete token-space diffusion.

Beyond continuous diffusion, discrete and sequence-level diffusion models such as D3PM [22], DiffuSeq [23], and continuous diffusion for categorical data [24] study diffusion-style generation over discrete or categorical text spaces. These works provide important contrasts to our approach: they modify the text generation process itself, whereas we study the failure modes of continuous latent refinement followed by parallel decoding.

## 2.2 Flow matching and Riemannian flow matching

Flow Matching [8], related to rectified-flow and optimal-transport conditional flow formulations [10, 11], trains a continuous normalizing flow by regressing a neural vector field onto a target vector field along a probability path from noise to data:

$$\mathcal{L}_{\text{FM}} = \mathbb{E} [\|v_{\theta}(z_t, t) - u_t\|^2], \quad u_t = z_1 - z_0 \quad (9)$$

Riemannian Flow Matching [9] extends this idea by defining vector-field matching under a manifold metric. This work uses the flow-matching view in a latent text space and adds a learned diagonal metric preconditioning. Rather than computing true Riemannian geodesics — which would require knowledge of the BERT latent manifold’s exponential map and connection — MetricNet learns a diagonal preconditioning matrix  $G_{\psi}$  that reweights the force-matching objective in decoder-sensitive directions:

$$\mathcal{L}_{\text{force}} = \mathbb{E} [\|f_{\theta}(z_t, t, z^p) - G_{\psi} \cdot u_t\|^2], \quad v_{\text{nat}} = G_{\psi}^{-1} f_{\theta} \quad (10)$$

The diagnostic result is cautionary: metric preconditioning improves latent geometry but cannot substitute for a decoder-readable start distribution, because the decoder basin is a discrete decision boundary that no smooth metric can fully approximate.

## 2.3 Latent diffusion and structured starts

Latent Diffusion Models [16] show that generative modeling can be made more efficient by operating in the latent space of an autoencoder. Most closely related to our setting, COSMOS [32] addresses latent decodability for text diffusion by training the autoencoder jointly for token-level reconstruction and alignment with frozen pretrained encoder activations, producing a compressed and smoother latent space for diffusion. Segment-Level Diffusion [17] addresses long-form text generation through segmentation and adversarial latent smoothing; like COSMOS, it engineers a more decodable latent space rather than characterizing the decodability failure mode directly. Our work is complementary to both: rather than primarily proposing a smoothed autoencoder space, we empirically characterize the decodability failure mode itself, showing that geometric proximity in latent space does not necessarily imply token recoverability under a parallel decoder. This contrast motivates a further question: whether pretrained-encoder alignment alone is sufficient to widen the decoder-readable basin for fully non-autoregressive parallel decoding, a setting not directly evaluated by COSMOS.

SDEdit [18] provides a useful analogy for structured-start generation: rather than sampling entirely from noise, it starts from a structured guide and denoises toward the data manifold. The present system follows a related principle for text: a rough continuation draft is encoded into latent space and then refined. Unlike SDEdit’s continuous image domain, text requires the refined latent to land precisely within the decoder-readable basin — the failure mode this work characterizes.

## 2.4 Non-autoregressive and iterative generation

Our work also relates to non-autoregressive and iterative generation. Early non-autoregressive translation models generated tokens in parallel using latent fertility variables [25], while Mask-Predict uses conditional masked language modeling for parallel refinement [26]. Levenshtein Transformer [27] and Insertion Transformer [28] further show that sequence generation can be framed as iterative editing rather than strict left-to-right decoding. Unlike these methods, our system performs refinement in a continuous BERT latent space and then evaluates whether the resulting states remain decoder-readable.

Text degeneration and decoding choices are also relevant to our diagnostics. Prior work shows that decoding strategy can strongly affect repetition and diversity [30, 31]. In our setting, argmax collapse is treated as a readout failure rather than as direct proof that the latent generator contains no useful structure.

# 3 Method

## 3.1 Stage-1 latent autoencoder

Let a token sequence be  $\mathbf{x} = (x_1, \dots, x_n)$  of length  $n$ . A frozen BERT encoder [2] maps tokens into contextual hidden states:

$$\mathbf{h} = E_{\text{BERT}}(\mathbf{x}) \tag{11}$$

A projection layer  $P$  maps hidden states into a continuous latent sequence:

$$\mathbf{z} = P(\mathbf{h}), \quad \mathbf{z} \in \mathbb{R}^{n \times d} \tag{12}$$

where  $d$  is the latent dimension ( $d = 768$  in our main experiments,  $d = 256$  for the compressed baseline). A parallel decoder  $p_\phi$  predicts all token distributions simultaneously:

$$p_\phi(x_i | \mathbf{z}) = \text{softmax}(D_\phi(\mathbf{z})_i) \tag{13}$$

The reconstruction objective is:

$$\mathcal{L}_{\text{AE}} = - \sum_{i=1}^n \log p_\phi(x_i | \mathbf{z}) \tag{14}$$

We evaluate both compressed 256-dimensional latents and full 768-dimensional BERT latents. The 768-dimensional setting removes the projection bottleneck as much as possible while keeping the same decoder interface.

## 3.2 Conditional latent flow matching

The latent sequence is split into prompt and suffix parts at position  $m$ :

$$\mathbf{z} = (\mathbf{z}^p, \mathbf{z}^s), \quad \mathbf{z}^p = \mathbf{z}_{1:m}, \quad \mathbf{z}^s = \mathbf{z}_{m+1:n} \tag{15}$$

where  $\mathbf{z}^p \in \mathbb{R}^{m \times d}$  is the known prompt latent and  $\mathbf{z}^s \in \mathbb{R}^{(n-m) \times d}$  is the suffix latent to be generated. In our ROCStories experiments,  $m = 32$  prompt token slots and  $n - m = 32$  suffix token slots.

Following the flow-matching view [8], in the original Gaussian-start formulation, a path interpolates between noise and the real suffix latent:

$$\mathbf{z}_0 \sim \mathcal{N}(0, I), \quad \mathbf{z}_1 = \mathbf{z}^s \quad (16)$$

$$\mathbf{z}_t = (1 - t)\mathbf{z}_0 + t\mathbf{z}_1, \quad t \sim \mathcal{U}(0, 1) \quad (17)$$

where  $I$  is the identity matrix and  $t$  is the interpolation timestep. The target velocity is:

$$\mathbf{u}_t = \mathbf{z}_1 - \mathbf{z}_0 \quad (18)$$

FlowNet  $v_\theta$  predicts a conditional velocity field, and the basic flow-matching objective is:

$$\mathcal{L}_{\text{FM}} = \mathbb{E} \left[ \|v_\theta(\mathbf{z}_t, t, \mathbf{z}^p) - (\mathbf{z}_1 - \mathbf{z}_0)\|_2^2 \right] \quad (19)$$

Diagnostics showed this Gaussian-start formulation was insufficient: generated latents  $\hat{\mathbf{z}}^s$  could achieve high cosine similarity with real suffix latents while still decoding poorly:

$$\cos(\mathbf{z}^s, \hat{\mathbf{z}}^s) \approx 1 \not\Rightarrow P_{\text{target}}(\hat{\mathbf{z}}^s) \text{ is high} \quad (20)$$

where  $P_{\text{target}}$  is defined formally in Eq. 40.

### 3.3 Metric-aware local refinement

Rather than computing true Riemannian geodesics — which would require knowledge of the BERT latent manifold’s exponential map and connection — MetricNet learns a diagonal preconditioning matrix  $G_\psi$  that reweights the force-matching objective in decoder-sensitive directions:

$$G_\psi(\mathbf{z}_t, t, \mathbf{z}^p) \succ 0, \quad G_\psi \in \mathbb{R}^{d \times d} \text{ diagonal} \quad (21)$$

FlowNet is trained to predict a force/covector  $f_\theta \approx G_\psi \mathbf{u}_t$  rather than the velocity directly. The force target is:

$$f_{\text{target}} = G_\psi(\mathbf{z}_t, t, \mathbf{z}^p) \cdot \mathbf{u}_t \quad (22)$$

and the force-matching objective is:

$$\mathcal{L}_{\text{force}} = \mathbb{E} \left[ \|f_\theta(\mathbf{z}_t, t, \mathbf{z}^p) - G_\psi(\mathbf{z}_t, t, \mathbf{z}^p) \cdot \mathbf{u}_t\|^2 \right] \quad (23)$$

At inference, natural velocity is recovered by inverting the metric:

$$v_{\text{nat}} = G_\psi^{-1} f_\theta = \frac{f_\theta}{g_\psi} \quad (24)$$

and the ODE update becomes:

$$\mathbf{z}_{t+\Delta t} = \mathbf{z}_t + \gamma \cdot v_{\text{nat}}(\mathbf{z}_t, t, \mathbf{z}^p) \cdot \Delta t, \quad \gamma = 0.01 \quad (25)$$

A small regularizer keeps the metric near identity early in training:

$$\mathcal{L}_{\text{metric}} = \|G_\psi - I\|_F^2 \quad (26)$$

In the current implementation, MetricNet is a small MLP with input dimension  $2d + 2$ , hidden dimension 256, and output dimension  $d$ . The metric log values are bounded by 0.50, then exponentiated and normalized. For ROCStories with  $d = 768$ , MetricNet has 0.66M parameters. Later runs showed that MetricNet can learn nontrivial anisotropy, for example diagonal standard deviation around 0.38 and range approximately [0.47, 1.28]. However, this geometric improvement only gives modest decoder-level gains, confirming that metric preconditioning alone cannot substitute for a decoder-readable start distribution.

### 3.4 Draft-conditioned start distribution

Prompt-only generation is highly multimodal. One prompt can have many valid continuations, so a prompt-only latent prior can average over incompatible targets. We therefore use a rough draft  $r$  as an instance-level guide. The draft is encoded by the same frozen BERT encoder:

$$\mathbf{z}_{\text{draft}} = P(E_{\text{BERT}}(r)) \tag{27}$$

The DraftPrior is implemented as a denoising prior over suffix latents. The input draft latent is mixed with Gaussian noise:

$$\mathbf{z}_t = \alpha \mathbf{z}_{\text{draft}} + \sqrt{1 - \alpha^2} \epsilon, \quad \alpha = 0.7, \quad \epsilon \sim \mathcal{N}(0, I) \tag{28}$$

The model predicts a residual correction:

$$\mathbf{z}_{\text{start}} = \mathbf{z}_t + f_{\eta}(\mathbf{z}_t, \mathbf{z}^p, \alpha) \tag{29}$$

where  $f_{\eta}$  is the DraftPrior network and  $\mathbf{z}^p$  is the prompt latent. It is trained with a combined objective:

$$\mathcal{L}_{\text{DP}} = \mathcal{L}_{\text{CE}} + \lambda_1 \mathcal{L}_{\text{MSE}} + \lambda_2 \mathcal{L}_{\text{cos}} + \lambda_3 \mathcal{L}_{\text{norm}} \tag{30}$$

where the regularizers are defined as:

$$\mathcal{L}_{\text{MSE}} = \|\mathbf{z}_{\text{start}} - \mathbf{z}^s\|^2 \tag{31}$$

$$\mathcal{L}_{\text{cos}} = 1 - \cos(\mathbf{z}_{\text{start}}, \mathbf{z}^s) \tag{32}$$

$$\mathcal{L}_{\text{norm}} = (\|\mathbf{z}_{\text{start}}\|_2 - \|\mathbf{z}^s\|_2)^2 \tag{33}$$

The norm regularizer explicitly trains DraftPrior to match both the angle and magnitude of the real suffix latent — addressing the limitation of cosine similarity alone, which measures only angular agreement.

Architecturally, the DraftPrior uses an  $\alpha$  embedding, a position embedding, and four Transformer-style layers. Each layer has suffix self-attention, prompt cross-attention, and a feed-forward block. The model uses eight attention heads and a feed-forward hidden dimension of 512.

Draft corruption is simple: target tokens are dropped with probability 0.05 and are not replaced. This creates a noisy but structured draft. The goal is not prompt-only generation; the goal is to test whether the model can refine a decoder-readable but imperfect latent start.

The local FlowNet then refines  $\mathbf{z}_{\text{start}}$  rather than generating from pure Gaussian noise. The local refinement target is a small residual fraction of the full displacement:

$$\mathbf{u}_{\text{local}} = \rho(\mathbf{z}^s - \mathbf{z}_{\text{start}}), \quad \rho = 0.05 \tag{34}$$

The ODE update uses a small scalar  $\gamma = 0.01$  that prevents the flow from moving far enough to destroy the draft-conditioned decoder-readable structure.

### 3.5 Auxiliary fused readout, OT regularization, and residual refinement

Because raw latent movement often changes decoder CE only weakly, we also evaluate an auxiliary token head and fused readout:

$$\ell_{\text{fused}} = \ell_{\text{decoder}} + \beta \ell_{\text{aux}}, \quad \beta = 0.1 \tag{35}$$

where the two loss terms are:

$$\ell_{\text{decoder}} = - \sum_{i \in M} \log p_{\phi}(x_i | \mathbf{z}_T) \quad (36)$$

$$\ell_{\text{aux}} = - \sum_{i \in M} \log p_{\text{aux}}(x_i | \mathbf{z}_t) \quad (37)$$

and  $M$  is the set of valid target token positions. This readout is decoder-aware and is often more effective than moving the latent alone.

We additionally tested distribution-level alignment between refined suffix latents and real suffix latents using an optimal-transport-style loss:

$$\mathcal{L}_{\text{OT}} = \text{OT}(\hat{\mathbf{z}}^s, \mathbf{z}^s) \quad (38)$$

implemented with Sinkhorn OT when available and a sliced-Wasserstein-style fallback otherwise. Finally, we tested bounded residual refinement as an ablation:

$$\mathbf{z}_{\text{res}} = \mathbf{z}_{\text{ode}} + \lambda \tanh(R_{\omega}(\mathbf{z}_{\text{ode}}, \mathbf{z}^p)) \quad (39)$$

where  $\lambda > 0$  bounds the maximum refinement magnitude, ensuring  $\|\mathbf{z}_{\text{res}} - \mathbf{z}_{\text{ode}}\|_{\infty} \leq \lambda$ . These extensions are treated as ablations, not as the main result.

### 3.6 Full inference procedure

Algorithm 1 summarizes the complete draft-conditioned latent refinement pipeline at inference time.

---

#### Algorithm 1 Draft-Conditioned Latent Refinement

---

**Require:** prompt  $x^p$ , draft  $r$ , ODE steps  $T$ , scale  $\gamma = 0.01$

- 1:  $\mathbf{z}^p \leftarrow P(E_{\text{BERT}}(x^p))$  ▷ Encode prompt
- 2:  $\mathbf{z}_{\text{draft}} \leftarrow P(E_{\text{BERT}}(r))$  ▷ Encode draft
- 3:  $\mathbf{z}_0 \leftarrow \text{DraftPrior}(\mathbf{z}_{\text{draft}}, \mathbf{z}^p)$  ▷ Decoder-readable start
- 4: **for**  $t = 0, \Delta t, 2\Delta t, \dots, 1$  **do**
- 5:  $f_{\theta} \leftarrow \text{FlowNet}(\mathbf{z}_t, t, \mathbf{z}^p)$  ▷ Predict force
- 6:  $v_{\text{nat}} \leftarrow f_{\theta} / G_{\psi}(\mathbf{z}_t, t, \mathbf{z}^p)$  ▷ Natural velocity
- 7:  $\mathbf{z}_{t+\Delta t} \leftarrow \mathbf{z}_t + \gamma \cdot v_{\text{nat}} \cdot \Delta t$  ▷ ODE step
- 8: **end for**
- 9:  $\hat{x} \leftarrow \arg \max p_{\phi}(\cdot | \mathbf{z}_T)$  ▷ Parallel decode

**Ensure:** token sequence  $\hat{x}$

---

## 4 Experimental Setup

### 4.1 Implementation Details

All experiments were conducted on a single NVIDIA RTX 4090 GPU with 24GB VRAM using PyTorch. Unless otherwise specified, models were trained with a fixed random seed of 1337. We report ROCStories experiments with full 768-dimensional BERT latents and a compressed 256-dimensional diagnostic baseline, maximum sequence length of 64, batch size up to 768, and up to 16-step ODE integration during inference. The implementation was maintained with a chronological change log recording architectural switches, evaluation fixes, and benchmark protocol changes; this

was especially important because several early rows were diagnostics rather than final comparable benchmark results.

Table 1 reports the main trainable component sizes for the compressed 256-dimensional configuration and the full 768-dimensional ROCStories configuration. FlowNet uses hidden dimension 512, depth 5, eight attention heads, depthwise convolution with kernel size 5, suffix self-attention, prompt cross-attention, and residual output heads. The ROCStories first2/last3 split uses 32 prompt slots and 32 target slots.

Table 1: Trainable component sizes in the current implementation.

Component	Compressed 256-d	ROCStories 768-d
DraftPrior	3.36M	23.84M
FlowNet	15.93M	27.74M
MetricNet	0.26M	0.66M

## 4.2 Dataset and split

We evaluate on ROCStories [5], where each example is a five-sentence commonsense story. We use a sentence-aware split:

$$\text{prompt} = \text{sentences 1-2}, \quad \text{target} = \text{sentences 3-5}.$$

The prompt and target are each allocated 32 BERT-token slots, giving a maximum length of 64 tokens. This avoids cutting prompts in the middle of sentences and better matches story continuation.

## 4.3 Draft corruption

For controlled refinement, the target continuation is corrupted to form a rough draft. The primary corruption is token dropout with no replacement. This setting is not prompt-only generation. It measures whether the model can refine a noisy structured draft back toward a decoder-readable continuation. We report 0%, 3%, 5%, and 10% dropout settings.

## 4.4 Metrics

For decoder recoverability we report cross-entropy (CE), average target-token probability  $p$ , and top-1 token accuracy under the frozen decoder. For text-level comparisons we report MAUVE [6], distinct-1/2, repetition rate, average generated length, latency per sample, and tokens per second. Diffusion-LM is discussed only as a literature reference unless explicitly reproduced under the same local ROCStories export, truncation, and scoring protocol. The reported Diffusion-LM MAUVE value is therefore not an apples-to-apples row in our benchmark tables. Because MAUVE is unstable with small sample counts and short continuations, the 500-sample MAUVE results should be interpreted as preliminary.

## 5 Results

### 5.1 DraftPrior corruption curve

Table 2 shows the main DraftPrior corruption curve. Moving from compressed 256-dimensional latents to full 768-dimensional BERT latents consistently improves recoverability. The improvement is not proportional to dimensionality; rather, it suggests that compression removes specific token-recovery information such as subword identity, rare words, and lexical choice.

Table 2: DraftPrior recovery on ROCStories under the first2/last3 split. Values are validation metrics under the frozen decoder.

Setting	Dropout	CE ↓	Target prob. ↑	Top-1 ↑
256-d latent	0%	0.39	0.87	0.89
256-d latent	3%	2.608	0.543	0.627
256-d latent	5%	3.165	0.434	0.525
768-d latent	0%	<b>0.235</b>	<b>0.938</b>	<b>0.944</b>
768-d latent	3%	<b>2.228</b>	<b>0.613</b>	<b>0.677</b>
768-d latent	5%	<b>3.069</b>	<b>0.483</b>	<b>0.573</b>
768-d latent	10%	4.112	0.272	0.357

The clean 768-dimensional setting is nearly decoder-readable. Mild corruption remains usable: 3% dropout reaches target probability 0.613 and 5% dropout reaches 0.483. At 10% dropout, performance drops sharply and qualitative samples show tail repetition and function-word loops. We therefore treat 10% as a stress-test regime rather than the main operating point.

### 5.2 Stage-2 local refinement

Table 3 summarizes representative 768-dimensional stage-2 validation snapshots using the 5% DraftPrior start. DraftPrior provides most recoverability. Raw local flow makes only small changes, while fused decoder-aware readout gives the clearest improvement. Scaling MetricNet and adding OT makes the metric nontrivial, but the decoder-level gain remains modest. A bounded residual refiner moves latents more, but did not improve the best validation recoverability in these runs. Figure 1 shows the corresponding training dynamics for a 3% draft-dropout 768-dimensional run.

Table 3: Representative 768-dimensional stage-2 refinement snapshots with a 5% DraftPrior start. Values come from validation diagnostics.

Stage / variant	CE ↓	Target prob. ↑	Note
DraftPrior start	3.193	0.457	Structured start
Raw local flow	3.219	≈0.46	Little direct gain
Fused readout	<b>2.904</b>	<b>0.493</b>	Best decoder-aware snapshot
Active MetricNet + OT	3.057	0.482	Nontrivial metric, modest gain
Bounded residual ablation	3.120	0.472	More movement, no clear gain
Oracle real latents	0.172	0.953	Frozen-decoder upper bound

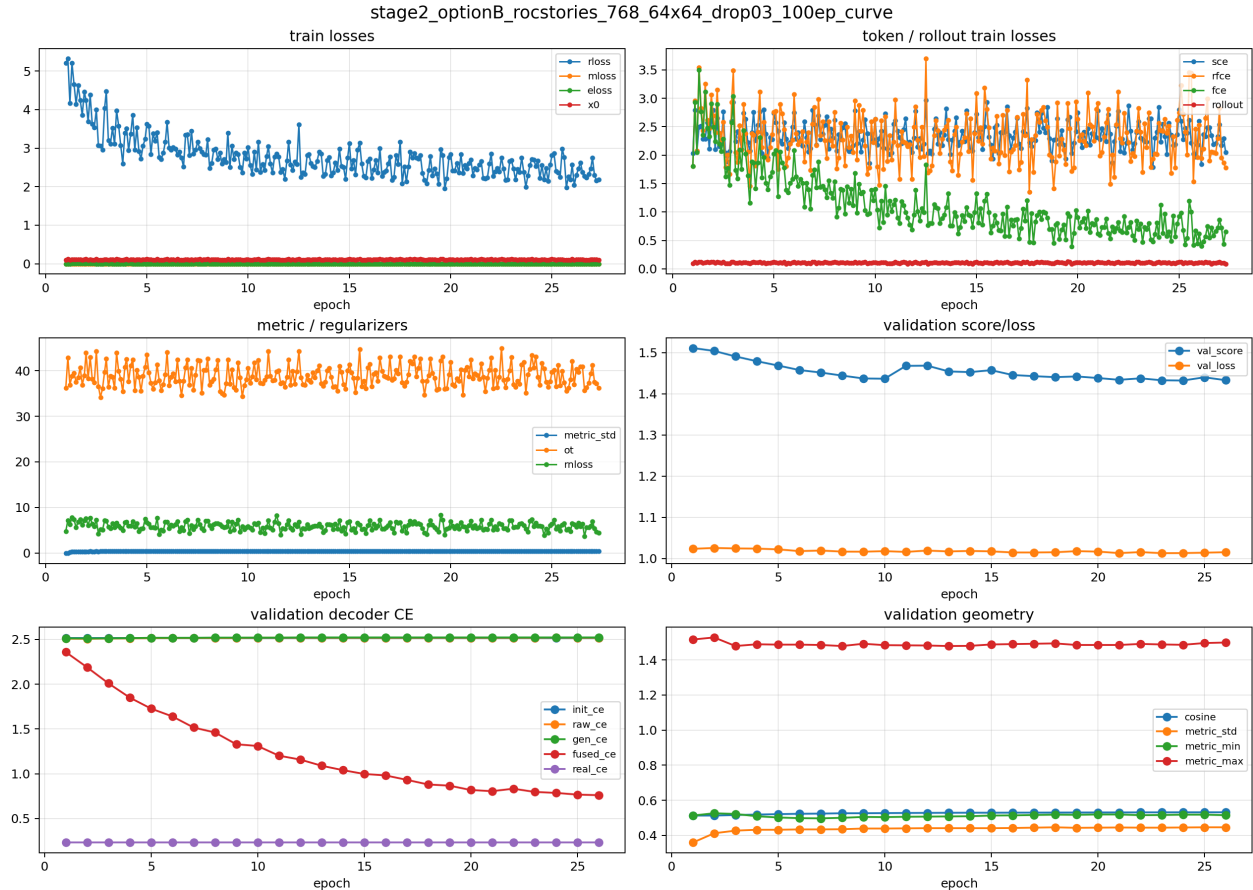


Figure 1: Stage-2 training dynamics for the ROCStories 768-dimensional 64/64 run with 3% draft dropout. The curve shows that decoder recoverability improves strongly for the fused readout, while the raw generated CE remains much worse than the real-latent decoder CE. This supports the paper’s main claim that local geometry and decoder-readable token recovery must be evaluated separately.

The gap to the oracle remains large. This shows that the remaining bottleneck is not merely latent distribution matching, but precise placement inside the decoder-readable basin.

### 5.3 Interpolation diagnostic

The interpolation diagnostic in Table 4 moves generated latents toward real latents:

$$\mathbf{z}_\alpha = (1 - \alpha)\hat{\mathbf{z}} + \alpha\mathbf{z}^s.$$

Small movement toward the real latent sharply improves CE, confirming that generated latents are in the right neighborhood but still outside the sharp decoder basin.

### 5.4 Quality-speed curve

Table 5 reports a preliminary 500-sample ROCStories quality-speed curve for the full 768-dimensional system using 64 fixed BERT suffix slots. The zero-step row corresponds to the DraftPrior-only output before ODE refinement. All rows in the table were produced by the local benchmark. The

Table 4: Interpolation diagnostic for 768-dimensional generated latents.

$\alpha$	0.01	0.03	0.05	0.10	0.20	0.50
CE ↓	3.188	3.123	3.057	2.885	2.482	0.589

commonly cited Diffusion-LM MAUVE value of 0.043 is a reported literature number, not a result from this local ROCStories benchmark, so it is excluded from the table and used only as background context.

Table 5: Preliminary 500-sample ROCStories quality-speed curve from the local benchmark only.

Model	Steps	MAUVE ↑	Dist-1 ↑	Rep. ↓	Latency ↓
Ours 768	0	0.0075	0.0323	0.0130	0.0034s
Ours 768	1	0.0062	0.0310	0.0123	0.0032s
Ours 768	2	0.0075	0.0316	0.0127	0.0033s
Ours 768	4	0.0068	0.0315	0.0121	0.0036s
Ours 768	8	0.0069	0.0311	0.0126	0.0040s
Ours 768	16	0.0074	0.0314	0.0111	0.0050s

A separate sentence-split local comparison gives GPT-2 autoregressive MAUVE 0.0067 and the 16-step 768-dimensional draft-conditioned system MAUVE 0.0109 under the same exported ROCStories rows. This comparison should still be read cautiously because GPT-2 is prompt-only autoregressive generation, while our system is synthetic-draft-conditioned latent refinement.

These results are not a state-of-the-art claim. They show that the controlled synthetic-draft system is not random, but its absolute MAUVE remains low. The main value of the report is the diagnostic analysis of recoverability, not benchmark dominance.

## 5.5 Qualitative behavior

Table 6 shows representative samples across three behavioral regimes. Near-perfect recovery occurs at short-to-medium target lengths (15–25 tokens): the system recovers event structure and most lexical content, with errors limited to dropped leading tokens or tail artifacts. Partial recovery at medium lengths (25–32 tokens) shows semantic near-synonyms replacing target words (“toppled” → “tumbled”, “pyramid” → “channel”, “faulty” → “failure”) and entity substitution (“conan” → “mickey”/“tom”). Full collapse occurs at longer targets ( $\geq 32$  tokens), where output degenerates into function-word loops. The 256-dimensional condition shows a qualitatively different failure mode: event scaffold is preserved but key nouns are wrong (“wide receiver” → “brand wave”, “play” → “class”), consistent with compression removing lexical specificity while retaining syntactic structure.

## 6 Failure Mode Analysis

### 6.1 Latent similarity is not discrete recovery

The central failure mode is that continuous similarity does not imply discrete recoverability. A generated suffix latent can be close to the real suffix latent under cosine similarity or MSE while

still lying outside the decoder decision region that produces the correct token:

$$\text{high } \cos(\mathbf{z}^s, \hat{\mathbf{z}}^s) \not\Rightarrow \text{high } P_{\text{target}}.$$

For a generated suffix latent  $\hat{\mathbf{z}}^s$ , define target-token probability as

$$P_{\text{target}}(\hat{\mathbf{z}}^s) = \frac{1}{|\mathcal{M}|} \sum_{i \in \mathcal{M}} p_{\phi}(x_i | \hat{\mathbf{z}}^s) \quad (40)$$

where  $\mathcal{M}$  is the valid target-token mask. This recoverability metric is more informative than latent cosine alone.

## 6.2 Compression removes token-recovery information nonlinearly

The 768-dimensional results show that compression is not neutral. Compressing BERT [2] contextual states to 256 dimensions preserves some semantic scaffold but loses token-level information needed for exact recovery. This explains errors such as semantically plausible but lexically wrong substitutions. The improvement from 256 to 768 is not 3 $\times$ , but it is consistent across corruption levels.

## 6.3 Argmax collapse is a readout failure

When decoder logits are broad, argmax repeatedly selects tokens with slightly larger output bias, often punctuation, articles, or common function words. This can create the appearance of total collapse. Sampling from the same logits may reveal more structure. Argmax collapse should therefore be reported as a diagnostic, not as the only evaluation of the latent generator.

## 6.4 Moving more is not enough

Once the DraftPrior start is decoder-readable, large flow updates can damage it. The residual ablation confirms that simply adding more latent movement is not sufficient. The movement must be decoder-aligned. Similarly, OT regularization can make latent distributions more geometrically aligned without guaranteeing token recovery. This reinforces the main thesis: geometry helps only when it respects the decoder interface.

# 7 Limitations

This is a diagnostic technical report, not a claim that the system solves non-autoregressive text generation. The strongest current result is controlled draft-conditioned refinement. Synthetic corrupted drafts contain target-derived information and must not be described as prompt-only generation. A mature comparison still requires stronger baselines such as discrete diffusion [22], DiffuSeq [23], Mask-Predict [26], Levenshtein Transformer [27], insertion-based models [28], VQ/codebook latents, and externally generated drafts.

The Riemannian component should also be interpreted carefully. Larger MetricNet variants can learn nontrivial metric anisotropy, but current metric and OT experiments produce only modest decoder-level gains. The present claim is not that learned Riemannian geometry solves text generation. The claim is that decoder-readable starts are necessary before geometry can help.

Finally, fixed-length target slots can create tail artifacts after the semantic continuation has ended. Future evaluation should truncate at an end marker where possible and compute token metrics only over valid target positions.

## 8 Conclusion

This report began with a simple question: can conditional flow matching in BERT latent space generate text continuations non-autoregressively? The diagnostic answer is more subtle than yes or no. Pure Gaussian latent generation is too weak because it lacks instance-level token information and often falls outside the decoder-readable basin. Prompt-only priors also struggle because valid continuations are multimodal. Structured draft conditioning changes the problem: it provides a readable start latent, after which FlowNet and MetricNet can be treated as local refiners. Full 768-dimensional BERT latents improve recovery over compressed 256-dimensional latents, confirming that compression can remove token-level information needed for discrete decoding. The main lesson is that latent geometry is not enough. Continuous-latent text generation must be evaluated by discrete recoverability, start-distribution quality, and whether refinement preserves rather than destroys decoder-readable structure.

*Stage 1 status.* The latent autoencoder, DraftPrior, and recoverability diagnostics reported here are complete. Stage 2—stronger refinement models, externally generated drafts, and broader baselines—remains ongoing.

## References

- [1] Vaswani, A., Shazeer, N., Parmar, N., Uszkoreit, J., Jones, L., Gomez, A. N., Kaiser, L., and Polosukhin, I. (2017). Attention Is All You Need. *NeurIPS*.
- [2] Devlin, J., Chang, M.-W., Lee, K., and Toutanova, K. (2019). BERT: Pre-training of Deep Bidirectional Transformers for Language Understanding. *NAACL-HLT*.
- [3] Radford, A., Wu, J., Child, R., Luan, D., Amodei, D., and Sutskever, I. (2019). Language Models are Unsupervised Multitask Learners. *OpenAI Technical Report*.
- [4] Lewis, M., Liu, Y., Goyal, N., Ghazvininejad, M., Mohamed, A., Levy, O., Stoyanov, V., and Zettlemoyer, L. (2020). BART: Denoising Sequence-to-Sequence Pre-training for Natural Language Generation, Translation, and Comprehension. *ACL*.
- [5] Mostafazadeh, N., Chambers, N., He, X., Parikh, D., Batra, D., Vanderwende, L., Kohli, P., and Allen, J. (2016). A Corpus and Cloze Evaluation for Deeper Understanding of Commonsense Stories. *NAACL-HLT*.
- [6] Pillutla, K., Swayamdipta, S., Zellers, R., Thickstun, J., Welleck, S., Choi, Y., and Harchaoui, Z. (2021). MAUVE: Measuring the Gap Between Neural Text and Human Text using Divergence Frontiers. *NeurIPS*.
- [7] Chen, R. T. Q., Rubanova, Y., Bettencourt, J., and Duvenaud, D. (2018). Neural Ordinary Differential Equations. *NeurIPS*.
- [8] Lipman, Y., Chen, R. T. Q., Ben-Hamu, H., Nickel, M., and Le, M. (2023). Flow Matching for Generative Modeling. *ICLR*.
- [9] Chen, R. T. Q., and Lipman, Y. (2024). Flow Matching on General Geometries. *ICLR*.
- [10] Liu, X., Gong, C., and Liu, Q. (2023). Flow Straight and Fast: Learning to Generate and Transfer Data with Rectified Flow. *ICLR*.

- [11] Tong, A., Malkin, N., Huguet, G., Zhang, Y., Rector-Brooks, J., Fatras, K., Wolf, G., and Bengio, Y. (2024). Improving and Generalizing Flow-Based Generative Models with Minibatch Optimal Transport. *TMLR*.
- [12] Albergo, M. S., Boffi, N. M., and Vanden-Eijnden, E. (2023). Stochastic Interpolants: A Unifying Framework for Flows and Diffusions. *arXiv:2303.08797*.
- [13] Ho, J., Jain, A., and Abbeel, P. (2020). Denoising Diffusion Probabilistic Models. *NeurIPS*.
- [14] Song, Y., Sohl-Dickstein, J., Kingma, D. P., Kumar, A., Ermon, S., and Poole, B. (2021). Score-Based Generative Modeling through Stochastic Differential Equations. *ICLR*.
- [15] Nichol, A. Q., and Dhariwal, P. (2021). Improved Denoising Diffusion Probabilistic Models. *ICML*.
- [16] Rombach, R., Blattmann, A., Lorenz, D., Esser, P., and Ommer, B. (2022). High-Resolution Image Synthesis with Latent Diffusion Models. *CVPR*.
- [17] Zhu, Y., Lan, Y., and Cheng, X. (2024). Segment-Level Diffusion for Long-Form Text Generation. *arXiv preprint*.
- [18] Meng, C., He, Y., Song, Y., Song, J., Wu, J., Zhu, J.-Y., and Ermon, S. (2022). SDEdit: Guided Image Synthesis and Editing with Stochastic Differential Equations. *ICLR*.
- [19] Li, X. L., Thackstun, J., Gulrajani, I., Liang, P., and Hashimoto, T. B. (2022). Diffusion-LM Improves Controllable Text Generation. *NeurIPS*.
- [20] Lovelace, J., Kishore, V., Wan, C., Shekhtman, E., and Weinberger, K. Q. (2023). Latent Diffusion for Language Generation. *NeurIPS*.
- [21] He, Z., Sun, T., Wang, K., Huang, X., Qiu, X., and Tang, Q. (2023). DiffusionBERT: Improving Generative Masked Language Models with Diffusion Models. *ACL*.
- [22] Austin, J., Johnson, D. D., Ho, J., Tarlow, D., and van den Berg, R. (2021). Structured Denoising Diffusion Models in Discrete State-Spaces. *NeurIPS*.
- [23] Gong, S., Li, M., Feng, J., Wu, Z., and Kong, L. (2023). DiffuSeq: Sequence to Sequence Text Generation with Diffusion Models. *ICLR*.
- [24] Dieleman, S., Sartran, L., Roshannai, A., Savinov, N., Ganin, Y., Richemond, P. H., Doucet, A., Strudel, R., Dyer, C., Durkan, C., Hawthorne, C., Leblond, R., Grathwohl, W., and Adler, J. (2022). Continuous Diffusion for Categorical Data. *arXiv:2211.15089*.
- [25] Gu, J., Bradbury, J., Xiong, C., Li, V. O. K., and Socher, R. (2018). Non-Autoregressive Neural Machine Translation. *ICLR*.
- [26] Ghazvininejad, M., Levy, O., Liu, Y., and Zettlemoyer, L. (2019). Mask-Predict: Parallel Decoding of Conditional Masked Language Models. *EMNLP-IJCNLP*.
- [27] Gu, J., Wang, C., and Zhao, J. (2019). Levenshtein Transformer. *NeurIPS*.
- [28] Stern, M., Chan, W., Kiros, J., and Uszkoreit, J. (2019). Insertion Transformer: Flexible Sequence Generation via Insertion Operations. *ICML*.
- [29] Ghazvininejad, M., Karpukhin, V., Zettlemoyer, L., and Levy, O. (2020). Aligned Cross Entropy for Non-Autoregressive Machine Translation. *ICML*.

- [30] Holtzman, A., Buys, J., Du, L., Forbes, M., and Choi, Y. (2020). The Curious Case of Neural Text Degeneration. *ICLR*.
- [31] Vijayakumar, A., Cogswell, M., Selvaraju, R. R., Sun, Q., Lee, S., Crandall, D., and Batra, D. (2018). Diverse Beam Search for Improved Description of Complex Scenes. *AAAI*.
- [32] Meshchaninov, V., Chimbulatov, E., Shabalin, A., Abramov, A., and Vetrov, D. (2025). COSMOS: Compressed and Smooth Latent Space for Text Diffusion Modeling. In *Advances in Neural Information Processing Systems 38 (NeurIPS)*.

Table 6: Selected qualitative samples. **Ref** is the ground-truth continuation; **Pred** is the system output. Substitution errors are shown in *italics*; dropped tokens in [].  $L$  = target length in tokens.

Prompt	Ref	Pred	$L$
<i>Near-perfect recovery (768-d)</i>			
Joseph clipped his toe nails. They went flying across the room.	one hit his sister on the head. his sister was disgusted. she slapped him and pushed him out of the room.	[one] hit his sister on the head. his sister was disgusted. she slapped him and pushed him out of the room.,	24
Ann went to a movies. She took a seat in a front row.	her neighbor accidentally spit some coke on her pants. he apologized. they started a nice conversation.	[her] neighbor accidentally spit some coke on her pants. he apologized. they started a nice conversation. got	19
<i>Partial recovery — lexical substitution (768-d)</i>			
Kasey was a cheerleader. She was performing at a football game.	she climbed to the top of the cheer pyramid. but then she toppled to the ground! kasey was lucky not to be injured.	climbed to the top of the cheer <i>channel</i> . but then she <i>tumbled</i> to the ground! kasey was lucky not to be <i>bruised</i> and	26
Conan was a bright red headed man. He wanted to host a show.	the network decided it was time for him to get his own show. conan was ready to take on the role. conan loved his new job.	network decided it was time for to get his own show. <i>mickey</i> was ready to take on the role. <i>tom</i> loved. new job and show...	31
<i>Collapse — long target (768-d)</i>			
Jeff was at a red light. All of a sudden it turned green.	as he was getting ready to accelerate, a car bumped into him. he got ready to pull over to exchange information and call the cops.	he was getting ready to fast a car bumped an him as. got had to taking while the the a to a was.,. a he out t. ...	41
<i>Compression failure (256-d)</i>			
Josh was the quarterback. His team was down by six points.	on the last play, a wide receiver got open in the end zone. josh threw the ball but it went over the receiver’s head. josh felt bad.	the last <i>class</i> , a <i>brand wave</i> got open in the end zone. josh threw the ball but it went over the receiver’s head. josh bad for letting his team down.	36